

Atomic-Scale Friction and Its Connection to Fracture Mechanics

R.W. Carpick, E.E. Flater, K. Sridharan, D.F. Ogletree, and M. Salmeron

This paper presents a study of contact, adhesion, and friction for nano-asperities using atomic-force microscopy. Proportionality was observed between friction and true contact area, as well as agreement with continuum mechanics models at the nanometer scale, although several features unique to the nanoscale were also observed. The continuum models can be understood in the framework of fracture mechanics and are used to determine the fundamental tribological parameters of nanoscale interfaces: the interfacial shear strength and the work of adhesion.

INTRODUCTION

As devices shrink in size, the increased surface-to-volume ratio ensures that interfacial forces such as friction and adhesion play dominant roles. For example, in microelectromechanical systems, catastrophic failure often occurs due to adhesion, friction, and wear.^{1,2} Understanding these forces may allow such problems to be remedied, and these forces may be exploited for specific applications.³

There is no fundamental theory to explain or predict friction. Macroscopically, the friction force (F_f) is often linearly proportional to the normal force or load (L) via Amontons' Law, as shown in Equation 1, which defines the friction coefficient μ (all equations are shown in Table I). Macroscopic friction is strongly affected by roughness, wear, third-bodies, and tribochemistry.⁴

The atomic-force microscope (AFM) is an important tool for studying contact, adhesion, and friction in a fundamental way.⁵ A tip with a radius of ~ 10 – 100 nm is attached to a cantilever spring. At low loads, the tip can form a well-defined nanometer-scale single contact (an "asperity") with the sample. Proper tip characterization and instrument calibration are crucial.^{6–8} See the sidebar for experimental details.

RESULTS

Atomic-Lattice Stick-Slip

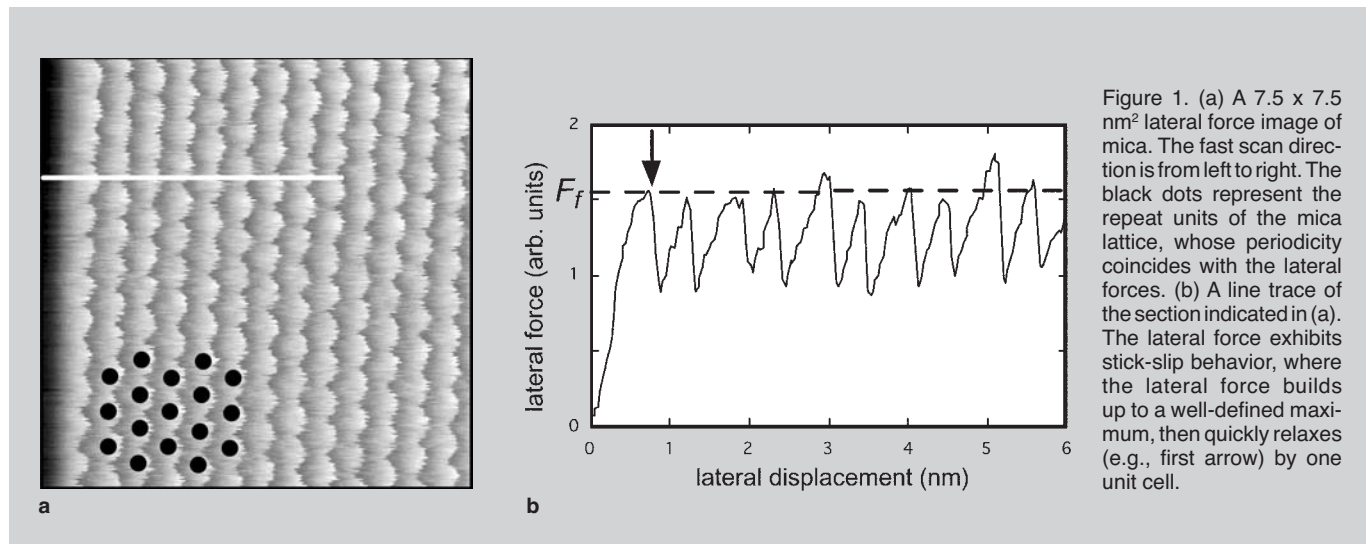
Atomic-force microscope tips in contact with crystalline samples often exhibit atomic-scale periodicity cor-

responding to the sample's lattice (Figure 1a).^{5,14} This results from discontinuous motion of the tip along the surface (Figure 1b). As the lever is rastered across the sample, the tip traces out the sample's lattice through a regular series of stick-slip events.¹⁴ The slip can be thought of as a fracture event: the interface ruptures and slips by one Burger's vector (the lattice constant). For the experiments here (see experimental details), stick-slip occurs for both mica experiments but not for SiN_x /diamond-like carbon (DLC), which is not surprising since both DLC and the SiN_x are amorphous.

There is a reproducible static friction force, F_f , at which the slip occurs (Figure 1b). To examine what determines F_f , the average value of F_f is measured for a series of loads.

Pt/Mica Interface: Friction as a Function of Load

For platinum/mica, friction is a non-linear function of load (Figure 2) in contradiction with Equation 1. A substantial negative load (the pull-off



force) must be applied to separate the interface. The data is well-fit by the Johnson-Kendall-Roberts (JKR)¹⁵ model for contact area between a paraboloidal tip and a plane. The JKR model balances elastic strain energy with adhesive interfacial energy to determine the contact area A , as shown in Equation 2, where R is the tip radius, γ is the work of adhesion, and E^* is the reduced Young's modulus of the tip and sample, where $E^* = ((1 - \nu_1^2)/E_1 + (1 - \nu_2^2)/E_2)^{-1}$. E_1, E_2 are the Young's moduli of the tip and sample respectively, and ν_1, ν_2 are the respective Poisson's ratios.

Since A varies with load in almost exact proportion to friction, Equation 3 is postulated, where τ is the interfacial shear strength. Equation 3 represents the essential relation governing friction for an elastic single asperity at this scale. The pull-off force L_c is related to the work of adhesion as shown in Equation 4.

Using bulk values for the elastic

constants ($E_{\text{mica}} = 56.5$ GPa, $\nu_{\text{mica}} = 0.098$,¹⁶ $E_{\text{Pt}} = 177$ GPa, and $\nu_{\text{Pt}} = 0.39$ ¹⁷), we solve for γ, τ , and the nanometer-scale contact radius (Table II). For platinum/mica, the values are for the maximum τ and γ observed; a gradual decrease of

both ensued due to contact-induced changes in the tip chemistry.¹² The adhesion energy is relatively strong, surpassing the range of the van der Waals' energy by an order of magnitude. Likewise, τ is extremely large. The theoretical prediction for the ideal shear strength of a perfect crystal (no dislocations) is $\sim G/30$ ¹⁸ where G is the shear modulus. An effective contact shear modulus is defined as $G_{\text{eff}} = 2G_{\text{mica}}G_{\text{Pt}}/(G_{\text{mica}} + G_{\text{Pt}}) \approx 22.3$ GPa. This gives, for platinum/mica, $\tau \approx G_{\text{eff}}/25$, comparable to the ideal shear strength.¹⁹

Limitations in Applying the JKR Model

Although the JKR model fits the friction data convincingly, the shear strength τ was assumed to be load-independent. In fact, load-dependent shear strengths have been observed in some cases.^{20,21} Furthermore, the JKR model assumes that the interfacial attraction has zero spatial range (i.e., it acts only when the materials are in contact.)²² This is appropriate only for compliant, strongly adhering materials with short-range attraction. The extreme opposite limit—stiff, weakly adhering materials with long-range forces—is described by the Derjaguin-Müller-Toporov (DMT) model.²³ Intermediate cases are treated by Maugis,²⁴ and a simplified form of Maugis' equations has been derived for practical use.^{25–27} For DMT and transitional cases, the variation of A with load significantly differs from the JKR solution.²⁸ Also, the JKR model assumes pure normal

EXPERIMENTAL PROCEDURES

Experiments were conducted at room temperature using either an ultrahigh vacuum (UHV) atomic-force microscope (AFM)⁹ or a Digital Instruments MultiMode AFM operating in nitrogen with controlled relative humidity. Commercial microfabricated cantilevers were used. Measurements of cantilever dimensions were combined with elasticity theory calculations to estimate the normal force spring constants, unless otherwise noted. The lateral force sensitivity was calibrated using the wedge technique.⁶ The tip geometry was experimentally determined to be nearly paraboloidal using inverse imaging.¹⁰

Three sets of interfaces are presented:

- A platinum-coated tip and a muscovite mica(0001) sample in UHV.^{11,12} The platinum coating was deposited by sputtering onto a plasma-cleaned silicon nitride cantilever. Muscovite mica was cleaved inside the UHV chamber, producing large step-free regions.
- A silicon nitride (SiN_x) tip and muscovite mica(0001) in UHV. The SiN_x cantilevers were used as-received and are partially oxidized.
- A SiN_x tip and a diamond-like carbon (DLC) thin film in a nitrogen environment, where the relative humidity was deliberately varied. The DLC films were deposited on silicon using a non-line-of-sight deposition technique known as plasma immersion ion implantation and deposition.¹³ The films have approximately 30–50% sp³ content and ~40 at.% hydrogen.

Table I. Equations

$$F_f = \mu \cdot L \quad (1)$$

$$A = \pi \left(\frac{3R}{4E^*} \right)^{2/3} \left(L + 3\pi\gamma R + \sqrt{6\pi\gamma RL + (3\pi\gamma R)^2} \right)^{2/3} \quad (2)$$

$$F_f = \tau \cdot A \quad (3)$$

$$\gamma = \frac{2L_c}{3\pi R} \quad (4)$$

$$k_{\text{contact}} = 8 \cdot G^* \cdot a \quad (5)$$

$$\frac{dF_{\text{lateral}}}{dx} = k_{\text{tot}} = \left[\frac{1}{k_{\text{lever}}} + \frac{1}{k_{\text{contact}}} \right]^{-1} \quad (6)$$

$$\frac{F_f(L)}{k_{\text{contact}}^2(L)} = \frac{\pi \cdot \tau(L)}{64 \cdot [G^*]^2} \propto \tau(L) \quad (7)$$

$$A = \pi \left(\frac{3R}{4E^*} \cdot (L + 2\pi R\gamma) \right)^{2/3} \quad (8)$$

$$\gamma = \frac{L_c}{2\pi R} \quad (9)$$

Table II. Solving for γ , τ , and Contact Radius Using Bulk Values for Elastic Constants

Interface	γ (mJ/m ²)	τ (MPa)	Tip Radius (nm)	Contact Radius @ L = 0 (nm)
Pt/mica	404	910	140	13.7
SiN _x /mica	24	52	260	8.4
SiN _x /DLC				
<5% RH	249	658	21	3.9
60% RH	255	906		4.0

loading, neglecting any effect from applied lateral forces.

Clearly, it is desirable to measure A directly. This is accomplished by measuring either the lateral contact stiffness^{29–33} or the contact conductance.^{34–36}

SiN_x/Mica Interface: Friction and Contact Stiffness as a Function of Load

Contact stiffness is the force-per-unit displacement compressing an elastic contact in a particular direction. It is measured in units of N/m and is essentially a “spring constant” of the contact. It applies both for normal and lateral displacements. The lateral contact stiffness of an axisymmetric contact, k_{contact} , is directly proportional to the contact radius a given by Equation 5,³⁷ where $G^* = [(2 - \nu_1)/G_1 + (2 - \nu_2 \pm 2 \pm)/G_2]^{-1}$. Here G_1 and G_2 are the tip and sample shear moduli, respectively. This convenient relationship holds for the JKR, DMT, or transitional regimes.

With AFM, the lateral contact stiffness exists in series with the lateral cantilever stiffness, k_{lever} . Thus, Equation 6 is true, where F_{lateral} is the lateral force and x is the lateral displacement. The slope of the initial sticking portion of the interaction during lateral sliding (Figure 1b) corresponds to $dF_{\text{lateral}}/dx = k_{\text{tot}}$, the total lateral stiffness. The measurement details are provided elsewhere.^{29–31,38}

A substantial variation of k_{tot} with load is observed for an SiN_x tip on a mica sample in UHV (Figure 3, crosses) due to the change in A. The JKR model, combined with Equations 5 and 6, describes A accurately (Figure 3, solid lines). Friction is also measured as a function of load (Figure 3, triangles), again agreeing with the JKR model. τ and γ , derived from the JKR fit, are listed in Table II. For these calculations, $E_{\text{SiN}_x} = 155$ GPa and $\nu_{\text{SiN}_x} = 0.27$ were

used. However, there is some uncertainty in these numbers.³⁹

The shear strength can be verified as load-independent without relying on the JKR analysis by simply dividing F_f at each load by the square of the corresponding contact stiffness (which is proportional to the contact area). By combining Equations 3 and 5, one obtains Equation 7. This is plotted in Figure 4, showing that τ is indeed load-independent over this range.

SiN_x/DLC Interface: Friction as a Function of Relative Humidity

Figure 5 shows F_f vs. load for a DLC film in a nitrogen environment of <5 and 60% RH, measured with an SiN_x tip. The normal force was calibrated in-situ using the resonance-damping method.⁸ An average value for the lateral sensitivity was determined from eight nominally identical cantilevers using the wedge method.⁶ To determine the RH dependence, a measurement was acquired at <5% RH, then a series of measurements (not shown) were acquired at progressively increasing RH, up to 60% (shown), then the RH was lowered again back to <5%. The data are highly consistent at each humidity.

Friction monotonically increases with humidity, but virtually no variation of the pull-off force is observed.

The data are in excellent agreement with Equation 4, but this time A is described by the DMT model (as shown in Figure 4, solid line),²³ which predicts that A should vary with load L as shown in Equation 8. Equation 9 shows that the DMT relation gives γ similarly to Equation 5. The average work of adhesion is ~ 0.25 J/m² (Table II).

The shear strength from Equations 3 and 8 increases by $\sim 40\%$, from 650–900 MPa, as the RH increases from <5% to 60%. Even the smallest value, 650 MPa, seems large for DLC, which is a low-friction material macroscopically. However, its low-friction mechanism involves the transfer of carbonaceous material to the counterface, producing a low-shear interface.⁴⁰ This experiment is in a completely different regime. Deformations are elastic, no observable transfer occurs, the counterface is oxidized silicon nitride, and friction is governed by adhesion and possibly atomic-scale contamination.

The RH-independence of γ conflicts with classical meniscus theory.⁴¹ While the interpretation of the structure of water at this scale is speculative, a minimum amount of water may be required for a meniscus, but it is hindered on the hydrophobic DLC. Water nonetheless has a significant effect. In molecular-dynamics simulations, arbitrary contaminants have a tendency to lock surfaces together and increase friction substantially.^{42–44} This effect may be occurring here.

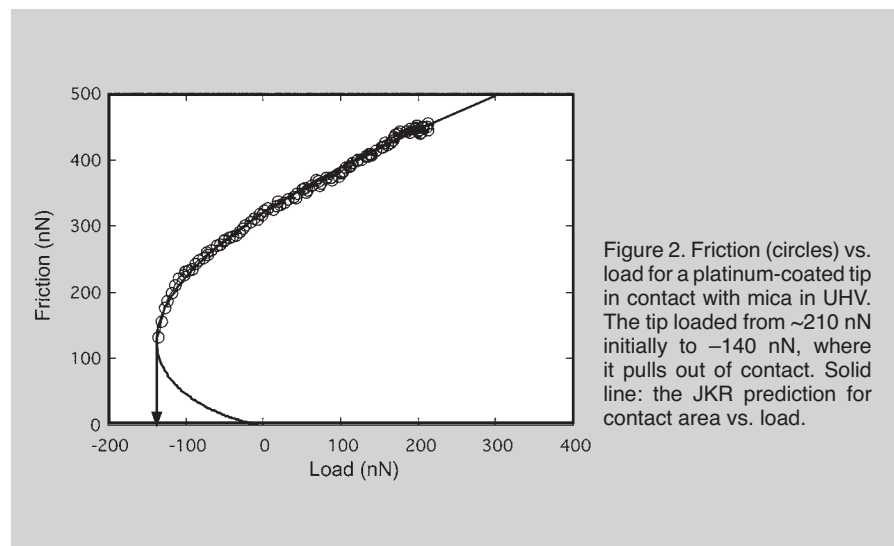


Figure 2. Friction (circles) vs. load for a platinum-coated tip in contact with mica in UHV. The tip loaded from ~ 210 nN initially to -140 nN, where it pulls out of contact. Solid line: the JKR prediction for contact area vs. load.

CONNECTIONS TO FRACTURE MECHANICS

In the previous examples, friction is proportional to the product of the true contact area and the interfacial shear strength. Either the JKR or DMT models of adhesive elastic contact provide excellent fits. A number of studies have shown agreement with Equation 3.^{5,11,12,29-35,45-49} However, the JKR and DMT models neglect tangential load, and there is no accounting for the specific mechanism of slip. To deal with these complications, fracture mechanics can be used.

The JKR model, for example, can be derived using fracture mechanics.^{50,51} The contact is considered as an external circular crack in an infinite medium. The contact edge represents the crack front. Loading and unloading corresponds to propagating this crack (advancing or receding) in mode I. Adhesion corresponds to attractive forces in a cohesive zone, and the load corresponds to the applied external separation force. Griffith's concept of brittle fracture is used to balance strain energy and

interfacial energy to solve for A as a function of load.⁵⁰ Maugis' transition model is derived from mode I fracture mechanics by using a Dugdale (square-well) cohesive zone model.²⁴

To account for tangential forces, Johnson⁵⁰ combined Maugis' model with interacting mode I, II, and III fracture. Johnson predicts that A is reduced by partial slip at the contact edge due to

lateral forces. Fitting the same data in Figure 2, he finds that the shape of the area-load relation still resembles the JKR curve, but has smaller values of A . He also predicts that lateral forces cause pull-off to occur at smaller loads compared with the pull-off force measured when not sliding. When this was tested experimentally, analysis for platinum/mica revealed an average reduction of L_c by ~ 0.89 due to sliding. Using this, τ increases by $\sim 20\%$ compared to the JKR fit for this model.

The near-ideal shear strength observed for platinum/mica is consistent with other experiments^{30,31,52} and remains to be explained. Modeling by Hurtado and Kim^{19,53} using dislocation mechanics suggests that below a critical nano-scale contact size, strongly adhered contacts exhibit ideal shear strengths because the contact is too small to allow even a single dislocation to nucleate at the contact edge. Dislocation nucleation reduces the shear strength substantially at larger scales. Experiments to test this model thoroughly are desirable.

CONCLUSIONS

Nanoscale single-asperity friction measurements consistently reveal that friction is proportional to the true contact area, frequently resulting in a non-linear dependence of friction upon load. Fracture mechanics provide a useful formalism for describing the relationship between contact area and load. These advances have shed new light onto the mechanics of nanoscale friction, and this can now be applied

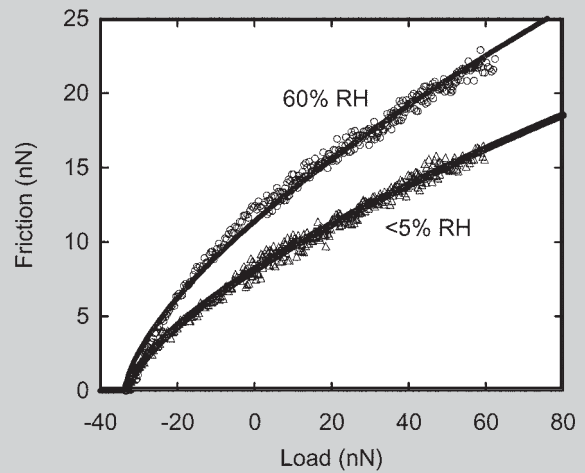


Figure 5. The friction vs. load at <5% (triangles) and 60% (circles) RH. Solid lines: DMT fits.

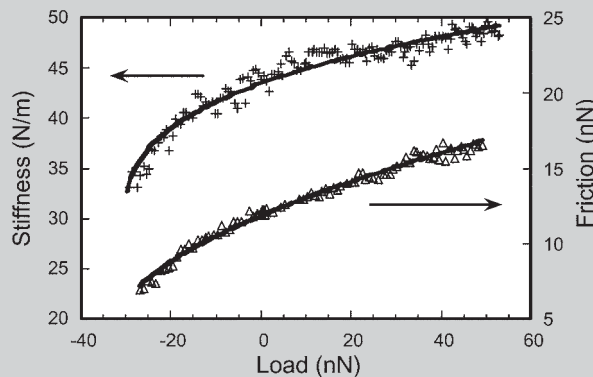


Figure 3. Crosses: lateral stiffness (k_{tot}) vs. load data for an SiN_x tip on mica in UHV. Triangles: F_f vs. load. Solid lines: fits of the JKR model.

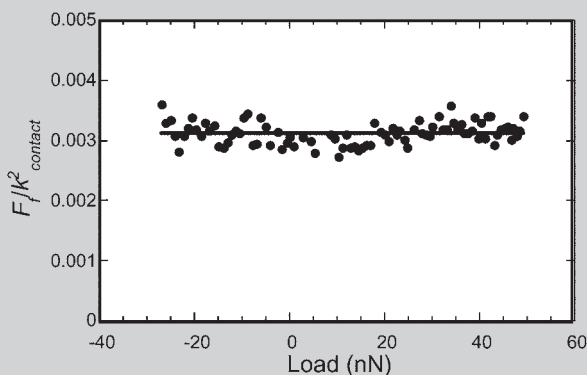


Figure 4. The $F_f / k_{\text{contact}}^2$ vs. load, calculated from the stiffness and friction data in Figure 3.

to the more challenging study of real, multi-asperity contacting interfaces such as those present in micromachine devices or macroscopic systems.

ACKNOWLEDGEMENTS

R.W. Carpick acknowledges support from the U.S. National Science Foundation (NSF) CAREER Program, grant #CMS-0134571, and from the U.S. Department of Energy (DOE), grant #DE-FG02-02ER46016. E.E. Flater acknowledges support from the NSF for a graduate research fellowship. D.F. Ogletree and M. Salmeron acknowledge the support of the Office of Energy Research, Office of Basic Energy Sciences, Material Science Division, of the DOE under Contract No. DE-AC03-76F00098.

References

1. R. Maboudian and R.T. Howe, *J. Vac. Sci. Technol.*, 15 (1) (1997), p. 1.
2. R. Maboudian, W.R. Ashurst, and C. Carraro, *Trib. Lett.*, 12 (2) (2002), p. 95.
3. M.P. de Boer et al., *J. Microelectromech. Syst.*, 13 (1) (2004), p. 63.
4. I.M. Hutchings, *Tribology: Friction and Wear of Engineering Materials* (London: Edward Arnold, 1992).
5. R.W. Carpick and M. Salmeron, *Chem. Rev.*, 97 (4) (1997), p. 1163.
6. D.F. Ogletree, R.W. Carpick, and M. Salmeron, *Rev. Sci. Instrum.*, 67 (9) (1996), p. 3298.
7. M. Varenberg, I. Etsion, and G. Halperin, *Rev. Sci. Instrum.*, 74 (7) (2003), p. 3362.
8. J.E. Sader, J.W.M. Chon, and P. Mulvaney, *Rev. Sci. Instrum.*, 70 (10) (1999), p. 3967.
9. Q. Dai et al., *Rev. Sci. Instrum.*, 66 (11) (1995), p. 5266.
10. J.S. Villarrubia, *Surf. Sci.*, 321 (3) (1994), p. 287.
11. R.W. Carpick et al., *J. Vac. Sci. Technol. B*, 14 (2) (1996), p. 1289.
12. R.W. Carpick et al., *Langmuir*, 12 (13) (1996), p. 3334.
13. S.M. Malik, R.P. Fetherston, and J.R. Conrad, *J. Vac. Sci. Technol. A*, 15 (6) (1997), p. 2875.
14. S. Morita, S. Fujisawa, and Y. Sugawara, *Surf. Sci. Rep.*, 23 (1) (1996), p. 3.
15. K.L. Johnson, K. Kendall, and A.D. Roberts, *Proc. Roy. Soc. London A*, 324 (1558) (1971), p. 301.
16. L.E. McNeil and M. Grimsditch, *J. Phys: Condens. Matter*, 5 (11) (1992), p. 1681.
17. J.R. Davis, ed., *Metals Handbook* (Metals Park, OH: ASM International, 1999).
18. A.H. Cottrell, *Introduction to the Modern Theory of Metals* (London, U.K. and Brookfield, VT: Institute of Metals, 1988).
19. J.A. Hurtado and K.-S. Kim, *Proc. Roy. Soc. London A*, 455 (1989) (1999), p. 3363.
20. B.J. Briscoe and D.C.B. Evans, *Proc. Roy. Soc. London A*, 380 (1779) (1982), p. 389.
21. I.L. Singer et al., *Appl. Phys. Lett.*, 57 (10) (1990), p. 995.
22. K.L. Johnson, *Langmuir*, 12 (19) (1996), p. 4510.
23. B.V. Derjaguin, V.M. Muller, and Y.P. Toporov, *J. Colloid Interface Sci.*, 53 (2) (1975), p. 314.
24. D. Maugis, *J. Colloid Interface Sci.*, 150 (1) (1992), p. 243.
25. R.W. Carpick, D.F. Ogletree, and M. Salmeron, *J. Colloid Interface Sci.*, 211 (2) (1999), p. 395.
26. O. Piétrement and M. Troyon, *J. Colloid Interface Sci.*, 226 (1) (2000), p. 166.
27. U.D. Schwarz, *J. Colloid Interface Sci.*, 261 (1) (2003), p. 99.
28. J.A. Greenwood, *Proc. Roy. Soc. London A*, 453 (1961) (1997), p. 1277.
29. R.W. Carpick, D.F. Ogletree, and M. Salmeron, *Appl. Phys. Lett.*, 70 (12) (1997), p. 1548.
30. M.A. Lantz et al., *Appl. Phys. Lett.*, 70 (8) (1997), p. 970.
31. M.A. Lantz et al., *Phys. Rev. B*, 55 (16) (1997), p. 10776.
32. O. Pietrement and M. Troyon, *Langmuir*, 17 (21) (2001), p. 6540.
33. O. Pietrement and M. Troyon, *Surf. Sci.*, 490 (1-2) (2001), p. L592.
34. M. Enachescu et al., *Phys. Rev. Lett.*, 81 (9) (1998), p. 1877.
35. M. Enachescu et al., *Trib. Lett.*, 7 (2-3) (1999), p. 73.
36. M.A. Lantz, S.J. O'Shea, and M.E. Welland, *Phys. Rev. B*, 56 (23) (1997), p. 15345.
37. K.L. Johnson, *Contact Mechanics* (Cambridge, MA: University Press, 1987).
38. O. Piétrement, J.L. Beaudoin, and M. Troyon, *Trib. Lett.*, 7 (4) (2000), p. 213.
39. C.J. Drummond and T.J. Senden, *Mater. Sci. Forum*, 189-190 (1995), p. 107.
40. A. Erdemir and C. Donnet, *Modern Tribology Handbook*, ed. B. Bhushan (Boca Raton, FL: CRC Press, 2001), Vol. 2, p. 465.
41. R.W. Carpick and J.D. Batteas, *Handbook of Nanotechnology*, ed. B. Bhushan (New York: Springer-Verlag, 2004), p. 1.
42. L. Wenning and M.H. Muser, *Europhys. Lett.*, 54 (5) (2001), p. 693.
43. G. He, M.H. Muser, and M.O. Robbins, *Science*, 284 (5420) (1999), p. 1650.
44. M.H. Muser, *Proceedings of the NATO Advanced Study Institute on Fundamentals of Tribology*, ed. B. Bhushan (Dordrecht, Netherlands: Kluwer Academic Publishers, 2001), p. 235.
45. A.R. Burns et al., *Langmuir*, 15 (8) (1999), p. 2922.
46. A.R. Burns et al., *Phys. Rev. Lett.*, 82 (6) (1999), p. 1181.
47. R.W. Carpick et al., *Fracture and Ductile vs. Brittle Behavior—Theory, Modeling and Experiment*, ed. G. Beltz, K.-S. Kim, and R.L. Selinger (Warrendale, PA: Mater. Res. Soc., 1999), p. 93.
48. R. Lüthi et al., *J. Vac. Sci. Technol. B*, 14 (2) (1996), p. 1280.
49. Z. Wei, C. Wang, and C. Bai, *Langmuir*, 17 (13) (2001), p. 3945.
50. K.L. Johnson, *Proc. Roy. Soc. London A*, 453 (1956) (1997), p. 163.
51. D. Maugis and M. Barquins, *J. Phys. D. (Appl. Phys.)*, 11 (14) (1978), p. 1989.
52. U.D. Schwarz et al., *Phys. Rev. B*, 52 (20) (1995), p. 14976.
53. J.A. Hurtado and K.-S. Kim, *Proc. Roy. Soc. London A*, 455 (1989) (1999), p. 3385.

In the print version of the journal,
this space presents an
advertisement for
Smart Imaging Technologies.
For more detail about this issue's
advertisers, review the
table of contents by visiting
<http://doc.tms.org/JOM/JOMDepartment>

R.W. Carpick, E.E. Flater, and K. Sridharan are with the Department of Engineering Physics at the University of Wisconsin in Madison, WI. D.F. Ogletree and M. Salmeron are with the Materials Sciences Division at Lawrence Berkeley National Laboratory in Berkeley, CA.

For more information, contact R.W. Carpick, University of Wisconsin at Madison, Department of Engineering Physics, 543 Engineering Research Building, Madison, WI 53706; (608) 263-4891; e-mail carpick@engr.wisc.edu.